A Computational Study of Flow Sensitivity of a PEM Fuel Cell with Multi-Parallel Flow Channels

M. A. Rahman[1], J. M. Mora[2], P. A. Chuang[1,*]
1. Thermal and Electrochemical Energy Laboratory (TEEL), Department of Mechanical Engineering, University of California, Merced, CA 95340, USA
2. University of Philippines-Diliman, Quezon City, Philippines
* Corresponding author: P. A. Chuang, Mechanical Engineering, University of California-Merced, CA 95340, USA, abel.chuang@ucmerced.edu

Abstract
In this paper, the effect of flow on water accumulation and the performance of a parallel flowfield based PEM fuel cell has been analyzed using a 3-D steady state, non-isothermal, single phase simulation model. Three flow conditions at 40°C are studied by the fuel cell model, which is developed using COMSOL Multiphysics. For the studied conditions, the simulation results show reduced water accumulation in flow channels and enhanced fuel cell performance when the flow rate is increased.

Keywords: PEM Fuel cell, Flow field, COMSOL, Parallel channel, Modeling.

Introduction
Fuel cell is an electrochemical energy conversion device that converts chemical energy directly to electricity. Most important aspect of a fuel cell is its clean nature, since the only two byproducts are heat and water. Fuel cells have been attracting a lot of attention as a feasible device to replace internal combustion engines for future transportation needs. Among the different types of fuel cells Polymer Electrolyte Membrane Fuel Cells (PEMFC) are expected to play the most crucial role due to its fast startup time and favorable power-to-weight ratio. Currently, PEM fuel cells are already in application in hybrid and full-electric vehicles [1,2], fixed wing unmanned aerial vehicle [3], power generations [4], and space missions [5].
The basic architecture of a PEMFC consists of an anode, proton exchange membrane, cathode, gas diffusion layer (GDL), and flow channels/bipolar plates. Even though fuel cell performance is mostly governed by its reaction kinetics at low current density, flowfield design play a very important role, especially at high current density. With a fixed membrane electrode assembly (MEA) and GDL, the performance of a fuel cell can largely be improved by an efficient flow field design at high current density. Flow fields, also known as Bipolar plates in stack, perform several crucial functions in fuel cell operation. These functions include supplying reactants to the reactions sites, effectively removing water generated by electrochemical reaction to prevent flooding, and providing structural support to the flimsy MEA. It also needs to be highly electronically conductive for collecting current.
Numerous research has been performed on individual channel cross sections of bipolar plates. Channels with rectangular cross sections are mostly used but trapezoidal, triangular, semi-circular profiles have also been investigated [6-8]. However, the overall design of flow fields and their orientation have a more significant impact on fuel cell performance. Conventional flow field designs include pin type, interdigitated, serpentine, parallel channel configurations [9,10]. Some researchers have also designed bio inspired flow fields [11]. Among these designs, parallel channels are considered to be a potential candidate for research due to its simplicity and the ability to uniformly distribute reactants. However, because of its low-pressure differential, parallel channel is also known to be susceptible for liquid water accumulation and blockage inside the channels, which is a severe drawback to this design. Increasing flow rate is often suggested in the literature as a feasible solution to overcome this problem. Thus, understanding the inlet flow sensitivity in parallel flow field design is a vital step to understanding and improving its performance.
In this study, a single phase, three dimensional, isothermal model has been developed to simulate the steady state performance of a PEM fuel cell with parallel flow fields. The cell operating conditions have been set to 40°C, 101.325 kPa and 50% relative humidity in both anode and cathode side. The effect of flowrate has been studied by analyzing the reactant and relative humidity distribution inside flow channels and cell performance through polarization and power density curves.

COMSOL Multiphysics Model

This fuel cell model has been developed assuming a steady state and isothermal operation. Isotropic properties are assumed for both electrode and membrane materials. The gas mixture in anode and cathode has been modeled as ideal gas. For the preliminary study, this model assumes that no water transportation is allowed across the membrane.

1. Geometry

The 3-D geometry of the parallel channel flow field and MEA assembly has been developed using the commercial CAD package SolidWorks 2016. The generated geometry was later imported in COMSOL using the CAD import module. Detail geometric parameters of the model are provided in table 1.

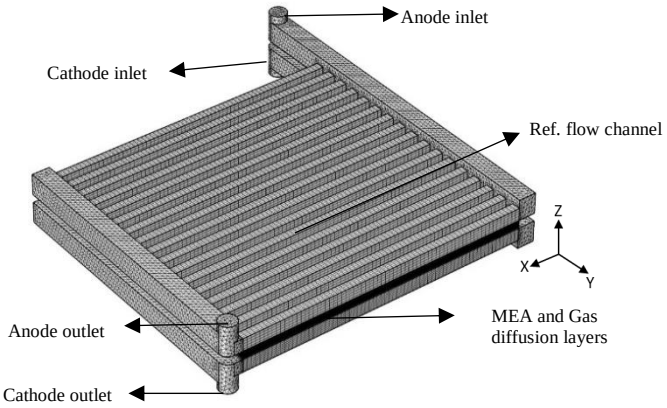

Figure 1 Computational Domain for simulation

2. Governing Equations

The "Secondary Current Distribution" interface has been used to model the electrochemical reactions in electrodes and the current distribution in MEA and GDL. Ohm's law and conservation of charge equation is solved in the electrochemistry domain which contains the MEA and GDL [13].

$$\begin{aligned} \nabla \cdot i_s &= -\sigma_s^{eff} \nabla \cdot \phi_s \\ \nabla \cdot i_s &= Q_s \\ \nabla \cdot i_l &= -\sigma_l^{eff} \nabla \cdot \phi_l \\ \nabla \cdot i_l &= Q_l \end{aligned} \qquad [1]$$

Here ϕ is the phase potential (l for electrolyte and s for electrodes), σ^{eff} is the effective conductivity $(\mathrm{S/m})$ and Q is the source term $(\mathrm{A/m^3})$. The subscript s is used to describe the solid electrode phase and "l" is for the membrane properties.

The sum of all reaction currents constitutes the source term "Q" in equation 1.

$$\begin{aligned} \nabla \cdot i_l &= \sum_m A_{v,m} i_{loc,m} \\ \nabla \cdot i_s &= -\sum_m A_{v,m} i_{loc,m} \end{aligned} \qquad [2]$$

Here A_v is the active surface area. Local current density i_{loc} for anode electrode is modeled using linearized Butler-Volmer equation and for cathode electrode it is modeled using cathodic Tafel approximation.

Table 1

Geometry Parameters	
Parameter	Value
Membrane/CL/GDL width	2.108 cm
Membrane/CL/GDL Length	2.013 cm
GDL Thickness	0.020 cm
Catalyst layer thickness	0.0025 cm
Membrane thickness	0.005 cm
Channel width	0.061 cm
Rib width	0.061 cm
Channel height	0.076 cm
Inlet/Outlet manifold width	0.127 cm
Inlet/Outlet manifold height	0.127 cm
Inlet manifold length	2.584 cm
Outlet manifold length	2.013 cm
Inlet diameter	0.127 cm
Outlet diameter	0.127 cm

$$i_{loc,anode} = i_0 \left[\frac{(\alpha_n + \alpha_c)F}{RT} \right] \eta_a$$

$$i_{loc,cathode} = -i_0 \times 10^{\eta_c / A_c}$$

To model mass transport "Transport of Concentrated Species" interface and to model momentum transport "Brinkman Equation" has been used. Navier-Stokes equation is used to solve the flow in gas channels and the Brinkman equation is used to describe the flow in porous regions. The dependent variables in the Brinkman equations are Darcy velocity and pressure [13].

$$\nabla \cdot (\rho \mathbf{u}) = Q_{br} \qquad [3]$$

Table 2

Operating Condition	
Temperature	40°C
Pressure	101.325 kPa
Humidity	50%/50%
Anode inlet flowrate	St 1, 5, 15
Cathode flowrate	St 1, 5, 15
Kinetic parameters	
Exchange current density HOR [12]	1×10^{5} A/m^2
Exchange current density ORR[12]	1 A/m^2
Anodic and cathodic Transfer coefficient	1
Material Properties	
Electrolyte conductivity[12]	9.825 S/m
Catalyst layer conductivity	222 S/m
GDL Porosity [12]	0.4
GDL Permeability [12]	1.18×10^{-11} (m^2)
Catalyst layer Porosity [12]	0.3
Catalyst layer Permeability [12]	2.36×10^{-12} (m^2)
Reactant gas properties	
$D_{O_2-N_2}$ (calculated)	2.47×10^{-5} (m^2/s)
$D_{O_2-H_2O}$ (calculated)	2.9×10^{-5}(m^2/s)
$D_{H_2-H_2O}$ (calculated)	9.47×10^{-5} (m^2/s)
$D_{N_2-H_2O}$ (calculated)	2.65×10^{-5}(m^2/s)
Mass fraction of H20 (cathode)	0.023
Mass fraction O2 (Cathode)	0.228
Mass fraction H2 (Anode)	0.743
Reversible cell voltage	1.229
Dynamic viscosity (Anode gas mixture) [12]	1.19×10^{-5} (Pa-s)
Dynamic viscosity (Cathode gas mixture) [12]	2.46×10^{-5} (Pa-s)

$$\frac{\rho}{\varepsilon_p}\left(\mathbf{u}\cdot\nabla\right)\frac{\mathbf{u}}{\varepsilon_p}= -\nabla p+\nabla\cdot\left[\frac{1}{\varepsilon_p}\left\{\mu(\nabla\mathbf{u}+(\nabla\mathbf{u})^{\mathrm{T}})-\frac{2}{3}\mu\left(\nabla\cdot\mathbf{u}\right)\mathbf{I}\right\}\right] -\left(\kappa^{-1}\mu+\frac{Q_{br}}{\varepsilon_p^2}\right)\mathbf{u}+\mathbf{F} \quad [4]$$

Here $\mathbf{u}$ is velocity of gas mixture, P is pressure, Q_{br} is the mass source and F is the influence of gravity.

$$\nabla\cdot\mathbf{j}_i+\nabla\cdot(\rho\omega_i\mathbf{u})=R_i \qquad N_i=\mathbf{J}_\mathbf{i}+\rho\mathbf{u}\omega_i \quad [5]$$

Multiphysics coupling between the electrochemistry and mass transport interface is achieved by coupling the reaction coefficients

$$R_{H_2}=-\frac{J_a}{2F}M_{H_2} \qquad R_{O_2}=-\frac{|J_c|}{4F}M_{O_2} \qquad R_{H_2O}=\frac{|J_c|}{2F}M_{H_2O} \quad [6]$$

$$\mathbf{j}_i=-\left(\rho\omega_i\sum_{k=1}^{Q}\tilde{D}_{ik}\mathbf{d}_k+D_i^T\nabla\ln T\right) \quad [7]$$

In equation 7, $\tilde{D}_{ik}(\mathrm{m}^2/\mathrm{s})$ are the multicomponent Fick diffusivities, ω_i is the mass fraction of species i, T (K) is the temperature, $D_i^T(\mathrm{Kg/m\text{-}s})$ are the thermal diffusion coefficients and $\mathbf{d}_k(1/\mathrm{m})$ is the diffusional driving force acting on reactant species. For idea gas mixtures, the diffusional driving force is defined as

$$\mathbf{d}_k=\nabla x_k+\frac{1}{p}\left[(x_k-\omega_k)\nabla p-\rho\omega_k\mathbf{g}_k+\omega_k\sum_{l=1}^{Q}\rho\omega_l\mathbf{g}_l\right] \quad [8]$$

Here, P is the total pressure, x_k is the mole fraction and M_n is mean molar mass. These are obtained by

$$x_k=\frac{\omega_k}{M_k}M_n \qquad M_n=\left(\sum_i\frac{\omega_i}{M_i}\right)^{-1} \quad [9]$$

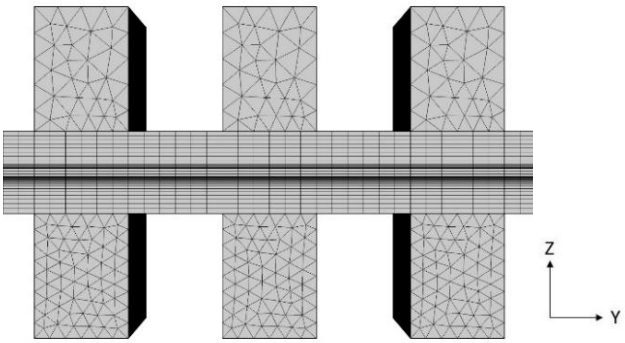

Figure 2 Physics controlled triangular mesh on flow channels and mapped rectangular mesh on diffusion layers, electrodes and membrane

Boundary Conditions:

Anode side of the cell was grounded and the cathode side was set to the cell potential. To solve the brinkman equation, inlet and outlet boundary conditions was set. Inlet velocity was calculated based on the stoichiometric flow rate required to generate 1 A/cm^2 from the fuel cell. Flowrate A, B and C in table 3 corresponds to stoichiometric flow of 1, 5 and 15 respectively at 1A/cm^2 current density. Table 3 shows the flowrates used for the simulation. Outlet was set to atmospheric pressure. For solving the mass transport equations inlet mass fraction was defined as the boundary condition.

Table 3

	Flowrate A (SLPM)	Flowrate B (SLPM)	Flowrate C (SLPM)
Anode Inlet	0.0416	0.208	0.527
Cathode Inlet	0.0736	0.368	0.932

Results:

The described fuel cell model developed using commercial FEA based solver COMSOL Multiphysics 5.3 is used to calculate fuel cell performance. Physics controlled tetrahedral mesh was generated in the intake and outlet manifold. In the YZ plane of the channel free triangular mesh was created with a maximum element size limit. In the GDL, CL and membrane user controlled 2D mapped mesh was created and later swept on to X direction. A segregated approach was used to solve each physics sequentially using the iterative solver GMRE (Generalized minimal residual method).

Operating conditions were set to 40°C, 101.325 kPa and 50% relative humidity at both anode and cathode. To analyze the effect of flowrate on reactant and water content distribution, the center (9th) channel from the inlet is taken as a reference. Figure 7 and 8 show the distribution of relative humidity in the reference channel at 0.7V and 0.4V, respectively. Since this is a single phase model, it is assumed that water is condensed to liquid form when the relative humidity exceeds 100%. At high current density and low flowrate (flow rate A), there is a high liquid water accumulation in the reference channel (Figure 8). Results show that 95% of the total channel length is filled with saturated water. As we increased the flowrate from A to C, liquid water is removed up to the half of channel length. At cell operating voltage of 0.7V (Figure 7), 78% of the channel length for flowrate At is filled with liquid water. Again, as the flow rate is increased the liquid water is removed from the channel. Figure 11 shows the 2-D surface plot of relative humidity distribution in cathode flow channel at 0.7V and 0.4V. The results further demonstrate that liquid water accumulation in parallel channel is very sensitive to flow rate and it can be reduced to a significant extent by increasing the flowrate.

Figure 5 shows Partial distribution of hydrogen in anode reference flow channel. Hydrogen distribution is more uniform anode side compared Oxygen cathode side. At a low flow rate (Flowrate A), hydrogen partial pressure drops from 96.5 kPa to 91 kPa. Whereas in cathode side, (Figure 6) oxygen partial pressure reduces to 0 kPa and creates oxygen depletion in catalyst layer. As the flowrate is increased to flow rate C, oxygen distribution becomes more uniform with a lower pressure drop. Figure 3 and 4, shows the overall performance of the fuel cell in a polarization plot and power density plot. The results indicate that with an increase in flowrate, the fuel cell performance is also improved. At flowrate A, limiting current behavior is observed due to reactant depletion in cathode catalyst layer.

In Figure 12 and 13, membrane current density in transverse to the parallel channel direction (Y direction) is plotted for flowrate A, B, and C. The wavy nature illustrates the land and channel distribution. In Figure 14, the current density along the parallel flow channel direction has been plotted. Results show that current density along flow channel direction is more uniform compared to the transverse direction. In transverse flow direction for all flow rates the current density curve shows a similar oscillating pattern. The peak of each oscillation occurs at the center of each flow channel where reactant supply is highest. But it can be observed from figure 14 that, the current density distribution along the flow channel direction becomes more uniform as flow rate is increased. At a low inlet flowrate (Flow rate A) the current density reaches close to zero near the exit due to oxygen depletion in cathode flow channels.

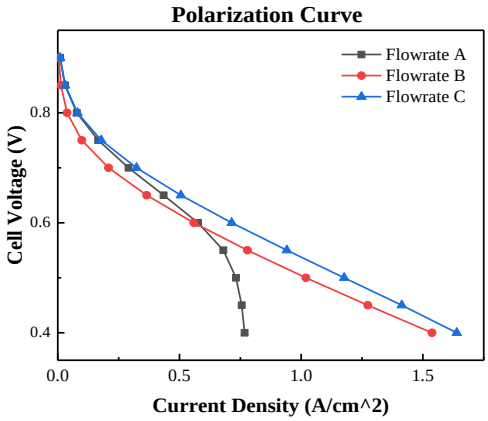

Figure 3 Polarization curve

Conclusion

A three-dimensional steady state isothermal model was developed to simulate PEMFC performance in low temperature operating conditions. The studied operating conditions are 40°C, 101.325 kPa, and 50% RH at both anode and cathode. The simulation was run in three constant flowrate conditions and the effects of flowrate on electrochemical reaction kinetics, reactant flow, diffusive and convective mass transport in flow channels, gas diffusion media and electrode are studied.

From this experiment it was found that, saturated water content in flow channel increases with increasing current density. The removal of liquid water from the channel is facilitated by increasing the flow rate. Power density and polarization curve results show that fuel cell performance is improved performance as flowrate is increased. Liquid water accumulation in channels is also reduced as flowrate is increased. Increasing flowrate provides a positive impact on overall fuel cell performance.

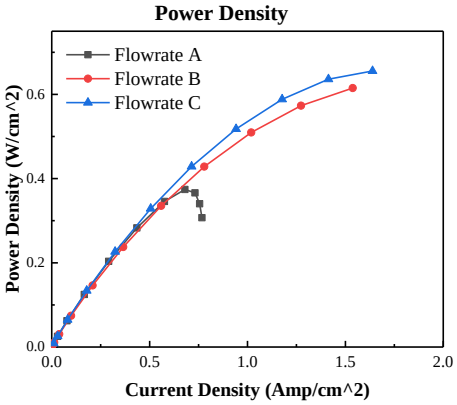

Figure 4 Power density curve at three different flow rates

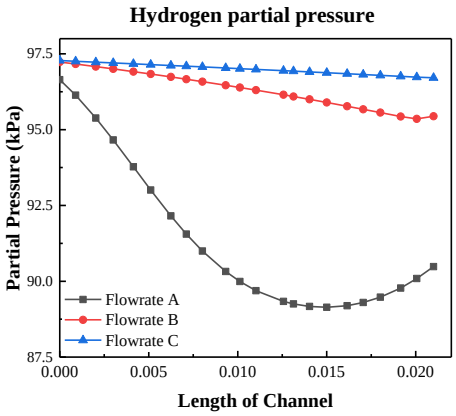

Figure 5 Hydrogen partial pressure in reference channel

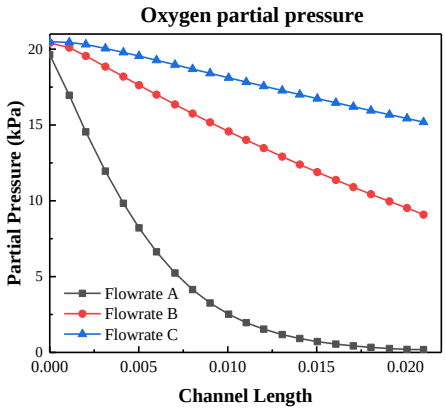

Figure 6 Oxygen partial pressure in reference channel

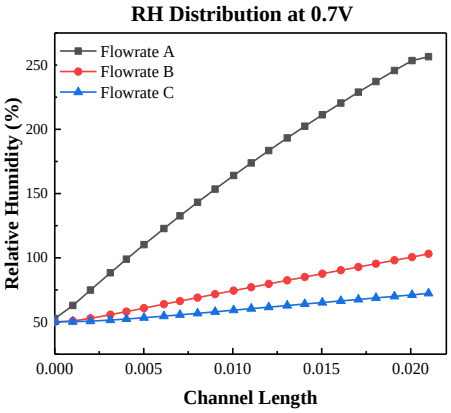

Figure 7 Relative humidity distribution in reference channel at 0.7V

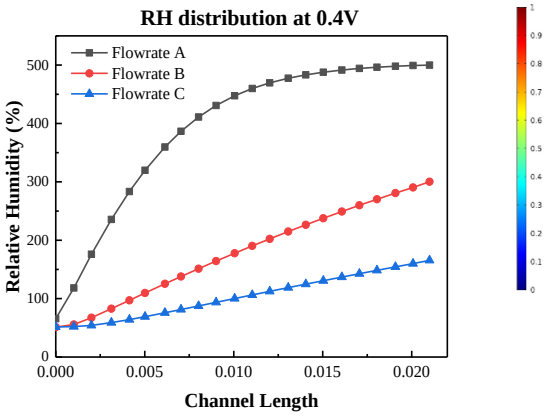

Figure 8 Relative humidity distribution in reference channel at 0.4V

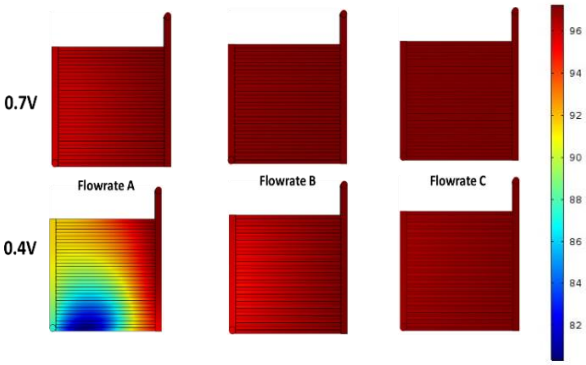

Figure 9 Hydrogen partial pressure (kPa) distribution on flow channels

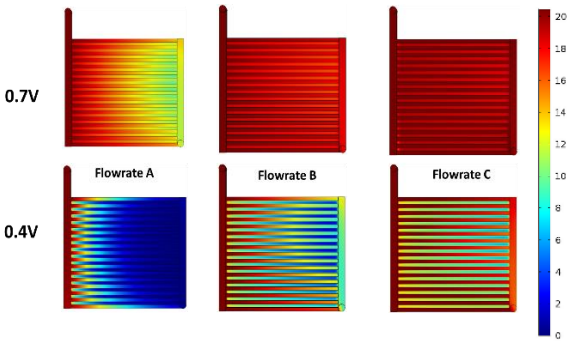

Figure 10 Oxygen partial pressure (kPa) distribution on flow channels

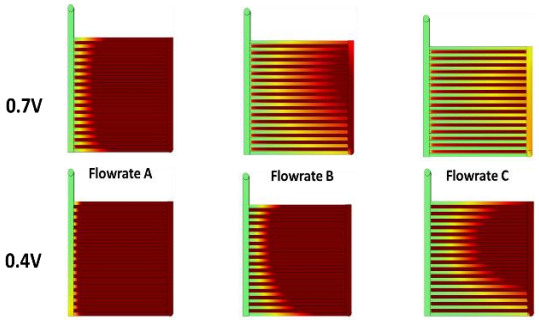

Figure 11 Relative humidity distribution in cathode flow channels at cell voltage 0.4 and 0.7V

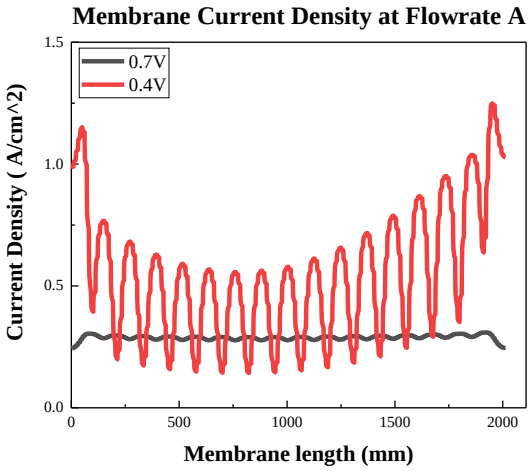

Figure 12 Membrane Current density in transverse to the parallel flow channel(Y direction) (A/cm^2) at Flowrate A

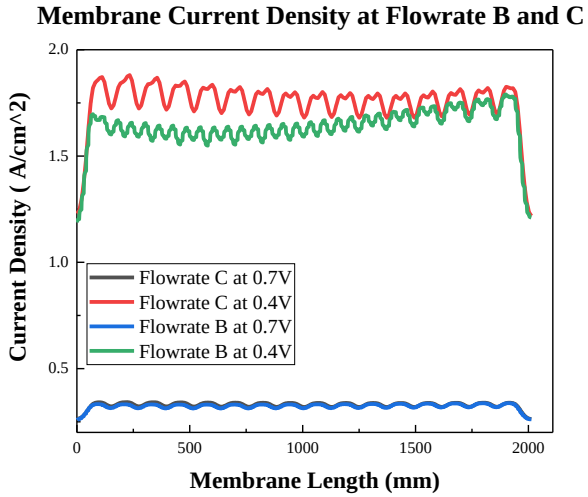

Figure 13 Membrane Current density (A/cm^2) in transverse to the parallel flow channel(Y direction) at Flowrate B and C

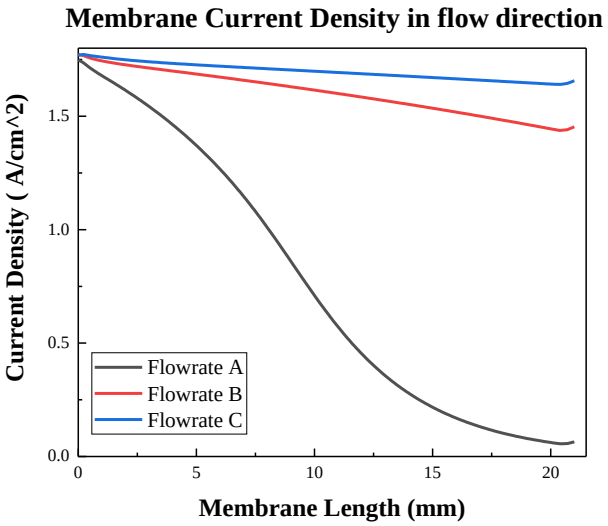

Figure 14 Membrane Current density in X direction (parallel to the flow channel direction) (A/cm^2)

Acknowledgements

The authors would like to acknowledge the GREENPower Program (IIID 2015-09) of the Commission on Higher Education – Philippine California Advanced Research Institutes (CHED-PCARI) of the Republic of the Philippines, and the University of California, Merced, USA for funding this research.

References

1. M. Ansarey, M.S. Panahi, H. Ziarati, M.Mahjoob, Optimal energy management in a dual-storage fuel-cell hybrid vehicle using multi-dimensional dynamic programming, *Journal of Power Sources*, **15**, 359-371 (2014)
2. T. Yoshida, K. Kojimaa, Toyota MIRAI Fuel Cell Vehicle and Progress Toward a Future Hydrogen Society, *Electrochemical Society Interface Summer 2015*, vol. 24, no. 2, pp. 45-49, (2015)
3. A. Gong, D, Verstraete, Fuel cell propuslsion in small fixed-wing unmanned aerial vehicles: Current status and research needs, *International Journal of Hydrogen Energy*, Volume **42,** Issue 33, pp. 21311-21333 (2017)
4. A. Choudhury, H. Chandra, A. Arora, Application of solid oxide fuel cell technology for power generation – A review, *Renewable and Sustainable Energy Reviews*, Volume **20**, 430-442 (2013)
5. P. Costamagna, S. Srinivasan, Quantum jumps in the PEMFC science and technology from the 1960s to the year 2000: Part II. Engineering, technology development and application aspects, *Journal of Power Sources*, vol. 102, no. 1-2, pp. 253-269, (2001)
6. A.P Manso, F.F. Marzo, M.G. Mujika, J. Barranco, A. Lorenzo, Numerical analysis of the influence of the channel cross-section aspect ratio on the performance of a PEM fuel cell with serpentine flow field design, *International Journal of Hydrogen Energy*, Volume **36**, pp. 6795-6808, (2011)
7. N.J. Cooper, A.D. Santamaria, M.K. Beckton, J.W. Park, Investigation of the performance improvement in decreasing aspect ratio interdigitated flow field PEMFCs, *Energy Conversion and Management*, Volume **136**, pp. 307-317 (2017)
8. A.L.R. Paulino, E.F. Cunha, E. Robalinho, M. Linardi, I. Korkischko, E.I. Santiago, CFD Analysis of PEMFC Flow Channel Cross Sections, *Fuel cells from fundamentals to systems*, Volume **17** issue 1, pp. 27-36, (2017)
9. X. Li, I. Sabir, Review of bipolar plates in PEM fuel cells: Flow-field designs, *International Journal of Hydrogen Energy*, Volume **30** Issue 4, pp. 359-371 (2005)
10. R. Boddu, U.K. Marupakula, B. Summers, P. Majumdar, Development of bipolar plates with different flow channel configurations for fuel cells, *Journal of Power Sources*, pp. 1083-1092 (2009)
11. A. Arvay, J. French, J.-C. Wang, X.-H. Peng, A.M. Kannan, Nature inspired flow field designs for proton exchange membrane fuel cell, *International Journal of Hydrogen Energy*, Volume **38**, Issue 9, 2013, Pages 3717-3726, ISSN 0360-3199
12. E. U. Ubong, Z. Shi,b, X. Wang, Three-Dimensional Modeling and Experimental Study of a High Temperature PBI-Based PEM Fuel Cell, *Journal of The Electrochemical Society*, **156** 10 B1276-B1282 (2009)
13. "Batteries and Fuel cell user's guide", COMSOL Multiphysics 5.3